Electronic Supplementary Material (ESI) for Journal of Materials Chemistry C.

A roadmap for laser optimization of Yb:$Ca_3(NbGa)_5O_{12}$–CNGG–type single crystal garnet

Jorge Omar Álvarez-Pérez, José María Cano-Torres, Ana Ruiz, María Dolores Serrano, Concepción Cascales and Carlos Zaldo*

Instituto de Ciencia de Materiales de Madrid. Consejo Superior de Investigaciones Científicas.

c/ Sor Juana Inés de la Cruz 3. 28049 Madrid. Spain.

*Corresponding author Email, cezaldo@icmm.csic.es

Electronic Supplementary Information

This page is intentionally left blank.

i) Laser achievements and laser setup

Table ESI.1 summarizes the laser achievements reported up to day for Yb:CNGG-type crystals.

In the present work to be close to the modelocking conditions, laser properties of the crystals were assessed in a z-shaped optical resonator sketched in Figure ESI.1. A TEM00 mode of a tunable cw titanium sapphire (Ti-sa) laser was used for optical pumping. Its emission wavelength was determined with an Angstrom interferometric wavelength meter, model HighFinesse WS/5, with a resolution of 0.01 nm. The pumping beam was focused by using a f= 80 mm lens through one of the cavity folding mirrors onto the uncoated samples. The pumping beam had good Gaussian profile, its diameter at the sample position was measured with a Thorlabs BP104-VIS slit scanning beam profiler as 62 μm, and the depth of focus amounts $2z_0 \approx 4$ mm. The two folding dichroic mirrors have a radius of curvature R=-100 mm, they are coated for high transmittance at λ= 800-985 nm and high reflectance at λ= 1010-1200 nm. The cavity back reflector and the output coupler were plane mirrors, the first with total reflection at pump and emission wavelengths and the output couplers with T_{OC}= 1, 2.5, 5 and 10% transmissions at the emission wavelength. Output and crystal transmitted light powers were measured with Gentec UP19K-15S-H5D0 and XLP12-3S-H2-D0 photodetectors. The laser output spectral distribution was obtained with ±0.2 nm resolution by using an APE laser spectrometer, model WaveScan, with λ= 1000-2600 nm spectral response. Uncoated samples were glued with silver paste to a water-cooled (16°C) copper holder. Samples were set perpendicularly to the pumping beam and the sample Fresnel reflections were evaluated from the refractive index of the crystals. Laser tuning was obtained by inserting a SF10 prism in the cavity, see Figure ESI.1.

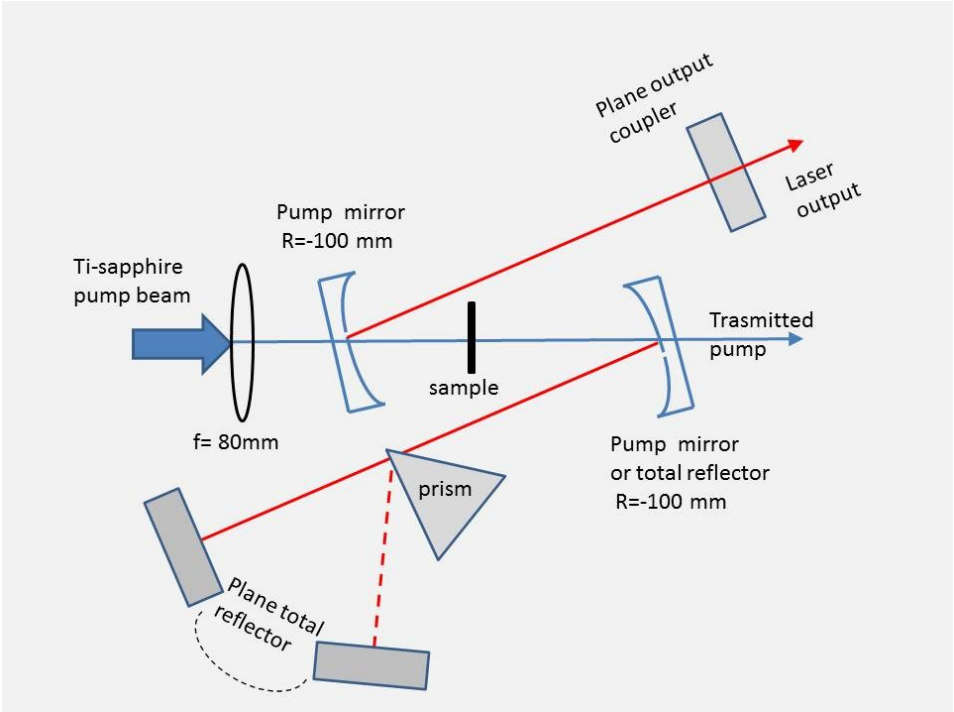

Figure ESI.1. Experimental setup used for characterization of cw laser operation.

ii) Laser report status.

Table ESI.1. Summary of spectroscopic and laser results reported for Yb:CNGG-type single crystals.

Crystal	Yb concentration at%		$\sigma_{ABS}/\lambda_{MAX}$ $10^{-20}cm^2/nm$	$\sigma_{ABS}/\lambda_{MAX}$/FWHM $10^{-20}cm^2/nm/nm$	$\frac{\sigma 972.5}{\sigma 932}$	Pump/ϕ nm/μm	Cavity type	d mm	$T_{OC}/\eta/\lambda_{EMI}$ %/%/nm	P_{ABS}/P_{OUT} W/W	τ μs	Ref
	Melt	crystal										
Yb:CNGG	5	5.77	1.6/934	3.3/973.5/3.5	2.1	DL, 974-975.5/--	PC		10/24.1/1037	7/1.25	791	1
Yb:CNGG	5	5.77	1.74/932	3.82/973.5/---	2.2	DL, 974-975.5/--	PC		10/40/--	2/0.6		2
Yb:CNGG	2.8		0.6/932	1.4/973/---	2.3			2	10/41/1032		780	3
Yb:CNGG	5		1.4/932	1.95/973/---	1.4	DL, 965-975/200	PC	1.5 2.5 3.5	10/61/1035 10/60/1042 10/70/1042	6.5/2.5 10/4.2 11/4.5		4
Yb:CNGG	5		1.4/932	2.2/---/---	1.4	DL/ 970-975/200	PC	3.5	10/63/1034	16/6.1		6
Yb:CNGG	5.8	5.73 $7.1x10^{20}$ cm^{-3}	0.9/932	1.8/973.5/4.4	2	DL, 930±10/104 DL,969/200	PC	8	10/37/1050 42	17/5 13/4.5		8
Yb:CNGG	5	5.77				Ti-sa,973.5/60	Z	2.5	10/23/1045.5	1.83/0.37		10
Yb:CLNGG	5			--/--/15	1	DL, 965-975/200	PC	2.18 3.14	10/77/1038 10/83/1038	6/3.5 8/5		5
Yb:CLNGG	5		1.5/932	2.2/---/---	1.6	DL, 970-975/200	PC	3.14	10/70/1034	15/7.6		6
Yb:CLNGG	5			---/---/7	1.37	DL, 965-973/200	PC	3.14	10/85/---			7
Yb:CLNGG	4.3	$5.3x10^{20}$ cm^{-3}	1.2/932	2.7/971.6/3.5	2.25	DL, 930±10/104 DL, 969/200	PC	3.14	10/54/1040 10/64/--	12/6 12/6		8
Yb:CLNGG	4.3		0.78/934	2.18/973/2.6	2.79							9
Yb:CLNGG	5					DBR DL, 979/---	Z	2.18	3/49/1045.1	0.5/0.16		11
Yb:CLNGG	5			2.18/973/2.6		DBR DL, 979/80	Z	2.18	5/48/--			12
Yb:CNNGG	10					DBT DL, 980/50	Z	3	5/68.5/--	1.6/0.734		13
Yb:CNNGG	10	11.9 $14.7×10^{20}cm^{-3}$	0.64/934	1.52/971.9/3.3	2.37	DL, 968/50	PP	3	2.5/56.5/1070	7.7/3.7	978	14
Yb:CLNNGG	10	10.7	0.64/934	1.3/971.9/3.3	2.03	DL, 968/50	PP	3	5/48/1059	7.3/2.73	1000	14

Continued. Laser modelocking

Crystal	Yb concentration at%		d mm	τ / λ_L /FWHM fs / nm / nm	<P_{OUT}> mW	f MHz	Pump/λ_P/T_{OC}/SAM - / nm /% / -	Ref
	melt	crystal						
Yb:CNGG	5	5.77	2.50	73 / 1047.5 / 19 94 / 1041 / 14.5 165 /1032 / 8.5	46 345 750	93	Tisa / 973.5 / 0.4 / SESAM- BATOP^R 1045nm / 3 / /10 /	10
Yb:CLNGG	5		2.18	90 / 1049 / 14 107 / 137 / 1039.3 /9.3	20 40 90	83	DBR-DL / 972 / 0.4 / SWCNT-SAM / 1 / / 3 /	12
Yb:CLNGG	5		2.18	55 / 1051.5 / 23 68 / 115 /	60 130 194	87	DBR-DL / 979 / 1 / SESAM 1030nm	11
Yb:CNNGG	10		3	45 / 1061 /26.8 62/1061 /26.8	30	104	DBR-DL / 980 / 0.8 / SESAM- BATOP^R 1064nm	13

PC= 2 plane-concave mirror cavity. PP= 2 plane mirrors cavity. Z=Astigmatically compensated 4 mirrors cavity. d= sample thickness. τ= $sech^2$ pulse duration. λ_P= Pump wavelength. λ_L= laser emission wavelength. <P_{OUT}>= average output laser power. f= repetition frequency. T_{OC}= output coupler transmission. Pump= Pump system. Tisa= titanium sapphire laser. DBR-DL= distributed Bragg reflector diode laser. SAM= saturable absorption mirror. SESAM= semiconductor saturable absorption mirror. SWCNT= single walled carbon nanotube saturable absorber.

References.

(1) H. Zhang et al, Opt Express 15, 9464, 2007. (2) J. Liu et al, Laser Phys. Lett, 5, 874-878, 2008. (3) V. E. Shukskin, Physics of Wave Phenomena 17(3) 165-191 2009. (4) Z. Zhou et al, Appl. Opt. 51, 4042, 2012. (5) J. Liu, Laser Phys. Lett. 9(5) 394-397, 2012. (6) J. Liu, Appl. Phys. B 109, 183-188, 2012. (7) Zhou Zhi-Chao et al, Phys Lett 29, 064212, 2012. (8) J. M. Serres et al, Opt. Mat. Express 6, 46-57, 2016. (9) V. Lupei, J. Appl. Phys. 112, 063110, 2012. (10) A. Schmidt et al, Opt. Comm. 283, 567-569, 2010. (11) Y. Zhang et al, Opt. & Laser Tech. 69, 144-147, 2015. (12) Y. Zhang et al, Opt. Express 22, 5635-5640, 2014. (13) Jie Ma et al, Opt. Express 25(13), 14968-14973, 2017. (14) Z. Pan et al, Solid State Lasers XXIX:Technology and Devices, Ed. W. A. Clarkson, R. K. Shori, Proc. SPIE 11259, 1125911, 2020.

iii) Crystal growth

As a preliminary step for crystal growth, the melting nature of $(Ca_{1-2x}Yb_xNa_x)_3(Nb_{0.3375}Ga_{0.6375})_5O_{12}$ precursor powders synthesized by solid state reaction (two steps of heating to 1330 °C for 6h with intermediate grinding) was studied by DSC, see Figure ESI.2. For undoped CNGG only a single endothermic peak was observed at 1442 °C upon two consecutive heating/cooling cycles, respectively, see Figure ESI.2a. This situation is basically maintained up to ≈20 at% of total Yb+Na cooperative substitution in the garnet formula, see Figure ESI.2b, although the garnet melting peak becomes less defined and shifts to lower temperatures, i. e. the garnet melting temperature is observed to decrease from 1442 °C to 1404 °C, and new endothermic peaks start to appear at about ≈20 at% of Ca substitution. For larger Ca substitutions new peaks at temperatures lower than that corresponding to the garnet melting are evidenced in the first and second DSC cycles, see Figure ESI.2c. These new phases melting at temperatures lower than those of the garnet may act as a flux for it, leading to the apparent temperature decrease of the garnet melt, but this melting down shift could be also related to the increasing Na content of the garnet phase. In any case for >40 at% of Ca substitution the DSC peak associated to the garnet cannot be observed. Thus, although the congruent melting of the garnet phase may occur for Ca substitution somewhat larger than 20 at%, it can be anticipated that the total Na plus Yb limit for melt stability occurs for ≈20 at% of Ca substitution in the dodecahedral garnet position. For higher substitution levels the products used to grow CNGG may contain only residual amounts of garnet phase. In fact for Ca substitution equal or larger than 90 at% the synthesized products do not melt completely suggesting the presence of a phase with melting above 1500 °C.

Ordered by increasing temperature the following non-garnet-related endothermic DSC peaks are observed, see Figure ESI.3: i) A first one (labeled PH1) appears only in the 2nd DSC cycle from 1270 °C to 1295 °C with increasing Ca substitution, ≥25 at% Na+≥25 at% Yb, it seems likely that it arises from the melting/decomposition of later described phases. ii) A second one (labeled as PH2) is seen both in the 1st and 2nd cycles at a nearly constant temperature, from 1329 °C to 1324 °C, it presumably corresponds to a compound with congruent melting. iii) Finally, another one (labeled as PH3) is observed only in the 1st cycle at decreasing temperature, from 1377 °C to 1327 °C, with increasing Ca substitution, ≥10 at% Na + ≥10 at% Yb, possibly its melting/decomposition is the origin of the secondary PH1 phase.

To identify the new phases contributing to the DSC thermal scans, parallel powder XRD analyses have been carried out. For a complete Ca substitution, i.e. nominally $(Na_{0.5}Yb_{0.5})_3(Nb_{0.3375}Ga_{0.6375})_5O_{12}$ powder mixture, the CNGG garnet phase is not observed, instead, a mixture of $Yb_3Ga_5O_{12}$ and $YNbO_4$ compounds is found, see Figure ESI.4a. The chemical stability of these phases may promote evaporation of unreacted $NaCO_3$. This situation also appears for 45 at% Na + 45 at% Yb of Ca substitution. In fact, $Yb_3Ga_5O_{12}$ is a garnet melting at 1725 °C,[1] thus within the operation range of our equipment it does not melt which agrees with our DSC observations.

For lower levels of Ca substitution the CNGG garnet phase is observed in the XRD scans but eventually mixed with other phases, see Figures SI.4b and SI.4c. $CaNbO_3$ is observed from 15 at% to 80 at% of Ca substitution, while the $CaYbNb_2O_7$ pyroniobate is formed from 20at% to 40 at% of Ca substitution. It seems to us likely that the pyroniobate phase decomposes into $CaNbO_3$

and $YbNbO_4$, thus a likely proposal for DSC phase assignments could be PH3= $CaYbNb_2O_7$, PH2= $CaNbO_3$ and PH1= $YNbO_4$.

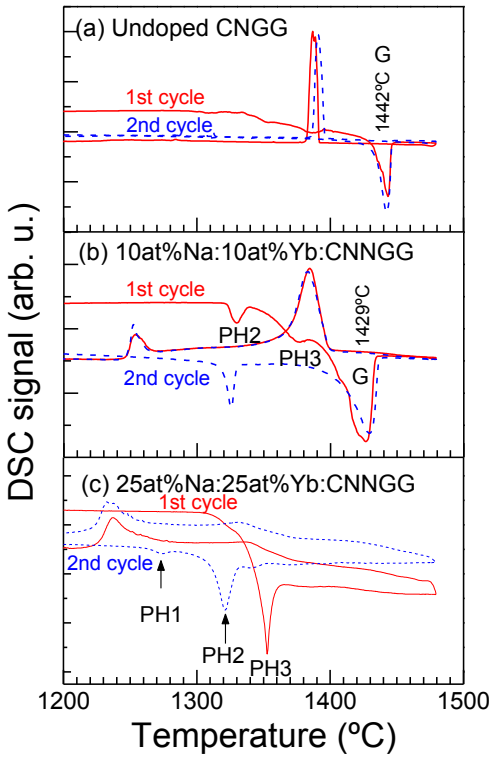

Figure ESI.2. DSC curves for ceramic (a) CNGG (b) 10 at% Na:10 at% Yb:CNNGG and (b) 25 at% Na:25 at% Yb:CNNGG powders.

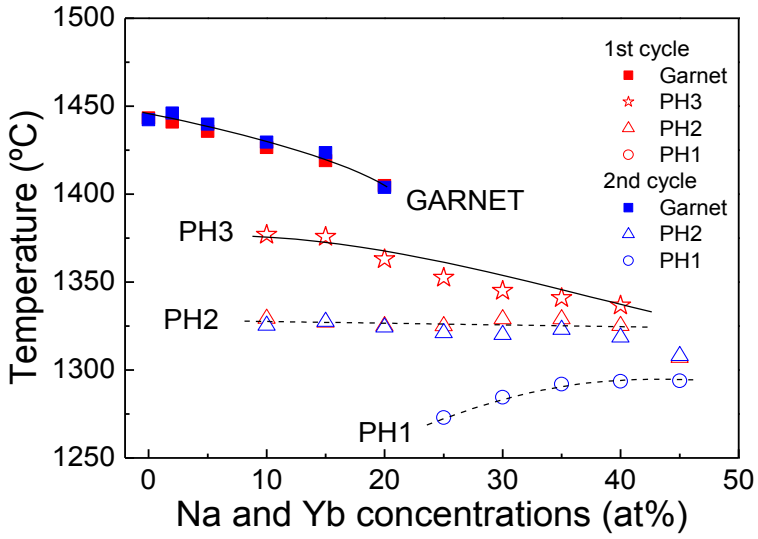

Figure ESI.3. Melting characteristics of $(Ca_{1-2x}Yb_xNa_x)_3(Nb_{0.3375}Ga_{0.6375})_5O_{12}$ ceramic powders observed by DSC. Full symbols correspond to the garnet melting, while open symbols are presumably associated with other crystallographic phases. Red and blue colors correspond to first and second DSC cycles, respectively. The lines are a visual help.

It is worth noting that $CaYbNb_2O_7$ and $CaNbO_3$ are also observed in the products of Yb:CNGG precursor powder and their presence is detected even at smaller Ca substitution levels than in the Na-modified Yb:CNNGG case. For instance, Figure 4d shows their presence in 10 at% Yb:CNGG synthesis. Thus Na modification contributes to the Yb:CNNGG garnet phase stability.

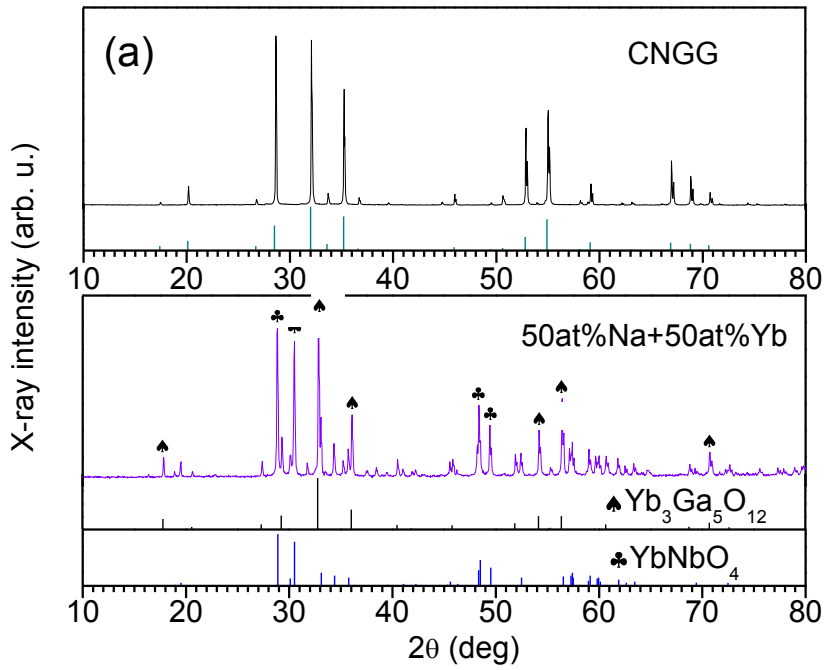

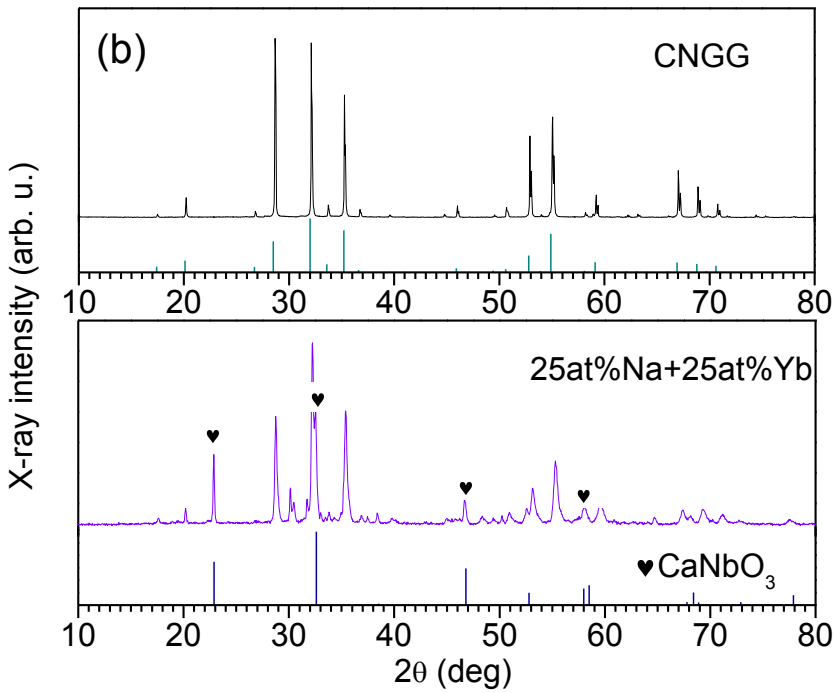

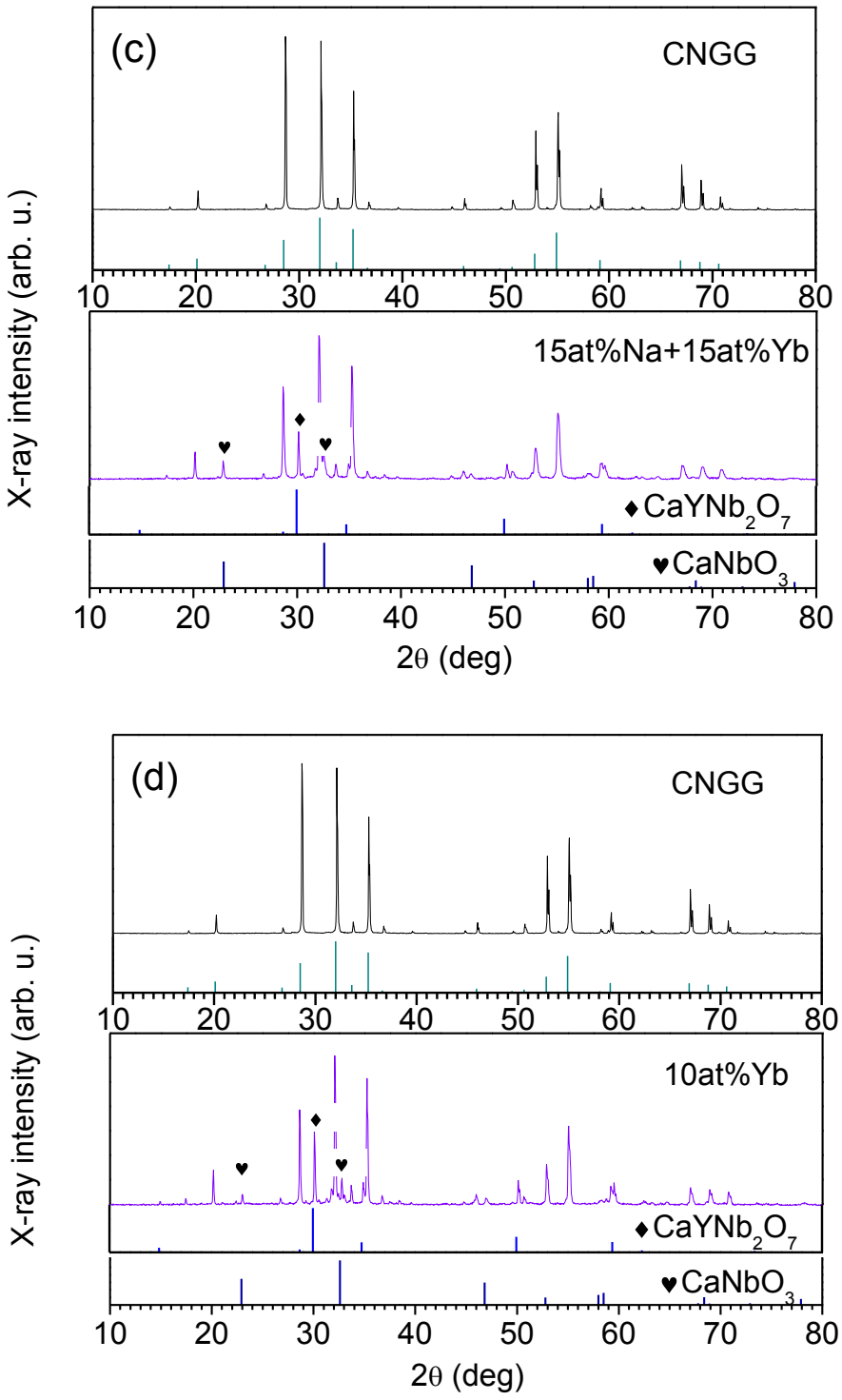

Figure ESI.4. XRD scans of Na:Yb:CNNGG and Yb:CNGG ceramic powders for different Ca substitution. The contributions of several compounds according to Inorganic Crystal Structure Database (ICSD) and Powder Diffraction Files (PDF) are given for reference: $Ca_3(Nb_{1.7}Ga_{0.2})Ga_3O_{12}$, ICSD 261821. $Yb_3Ga_5O_{12}$, PDF 73-1373. $YbNbO_4$, PDF 23-1480. $CaYNb_2O_7$ ICSD 50035-PDF 87-0022. $CaNbO_3$ ICSD 85569-PDF 89-0718.

The melting nature of the grown CNGG-type crystals was also studied by DSC. The endothermic and exothermic peaks observed are narrow in all crystals and reproducible after two melting/resolidification cycles, showing a good congruent melt. Table ESI.2 summarizes main results obtained. Undoped CNGG single crystal melts at 1438.7 ºC, i.e. slightly lower than the equivalent polycrystalline precursor synthesized by solid state reaction (1442ºC), this small change can be attributed to some slight composition modification due to selective melt evaporation during the growth process. Li incorporation rises the melting temperature by ≈10ºC. The Yb doping increases the melting temperature proportionally to the Yb content reaching temperatures above 1450ºC. Only Na modification is able to reduce the melting temperature of the crystals by 20-30ºC despite Yb doping.

Table ESI.2. Melting temperature (T_m) for different CNGG-type single crystals monitored by the maximum of the endothermic DSC peak.

	Modifier	Yb in crystal (at%)	T_m 1st cycle (°C)	T_m 2nd cycle (°C)
CNGG	none	0	1438.7	1438.9
Yb:CNGG	none	9.01	1445.0	1444.4
Yb:CNGG	none	12.07	1451.9	1450.7
CLNGG	Li	0	1448.2	1449.4
Yb:CLNGG	Li	7.57	1454.8	
Yb:CNNGG	8.78at%Na	7.13	1420.1	1421.1
Yb:CLNNGG	Li and 6.09at%Na	9.35	1435.1	1437.3

This page is intentionally left blank.

iv) Inventory of used crystals. Table ESI.3 summarizes all Yb:CNGG-type crystals used in this work and their relevant physical properties.

Table ESI.3. Yb:CNGG-type single crystals grown by Czochralski. $(Ca_{1-x-y}Na_xYb_y)_3Nb_{1.68}Ga_{3.2}\square_{0.12}O_{12}$ (x+y < 0.2) is the melt composition. Na and Yb concentrations in the crystal were measured either by EPMA ($^{@}$), WDXRF (*) or scXRD refinements ($^{+}$) and in some cases derived from OA meaurements ($^{\#}$). Reagent purity: 99.99% Ga_2O_3, others are specified with the following nomenclature, 2N= 99%, 2.5N= 99.5%, 3N= 99.9%, 4N=99.99% , 4.5N≥99.995% and 4.8N≥99.998%. Pulling and rotation rates are for the crystal neck (N), shoulder (Sh), body (B) and tail (T). Crystal color perceived by the naked eye under sun light illumination: G= green, Y= yellow, GY= greenish-yellow, LY= light yellow, CL= colorless. R-NIR is the integrated optical absorption in the Δλ= 800-550 nm range (nm×cm^{-1}). VIS is the optical absorption coefficient at λ= 400 nm (cm^{-1}). τ is the 300 K Yb^{3+} lifetime. Δθ is the FWHM of the *100* rocking curve. η= laser slope efficiency and P_{th}= pump power laser threshold for T_{OC}=10%.

Dopant composition In melt/crystal (at%/at%-10^{20} atcm^{-3})	Seed Atmosphere	Reagent purity	Pulling rate (mm/h)	Rotation rate (min^{-1})	Cooling rate (Δ% RF power → h)	Cell volume (Å^3)	Δθ (deg)	Color			τ (μs)	η_{qcw-cw}/ $P_{th,qcw-cw}$/ABS (%) / (mW) / (%)
								Eye	R-NIR	VIS		
Yb:CNGG												
Yb, 0			2	20	20.7-10 → 45 10-2 → 15	1951.67	0.0123	GY	30.8	1.06		
Yb, 0.3/0.08$^{\#}$-0.098	Pt Air	$CaCO_3$ 2.5N Nb_2O_5 3N, Yb_2O_3 4N	1.9	20	21-10 → 40 10-2 → 10	1951.67		Y	28.5	17.85	781	NO LASING
Yb, 8/9.65$^{@}$- *11.92*	111YAG Air	$CaCO_3$ 2.5N Nb_2O_5 3N, Yb_2O_3 3N	1.5(N) 1.8(Sh+B+T)	20	20.5-12 → 40 12-2.5 → 15	a=12.55 1976.65	0.01929 0.0378	G	60.3	3.33	484±50	57-46 / 167-130 / 77-63
Yb, 8/9.08$^{@}$ *-11.21*	111YAG Air	$CaCO_3$ 2.5N Nb_2O_5 3N, Yb_2O_3 4N	1.4(N) 1.5(Sh+B+T)	30(S+Sh+B) 25(T)	20.6-13 → 50 13-2.5 → 50	12.56(2)	0.02129	Y	30.9	12.14	547	60-71 / 53-82 / 70-62
Yb, 8/9.01$^{@}$ *-11.13*	Pt Air	$CaCO_3$ 4N Nb_2O_5 4N, Yb_2O_3 4N	1.2(N) 1.6(Sh+B+T)	20	22-10 → 45 10-0 → 15		0.04572	Y	7.79	7.93		75-77 / 76-76 / 78-71
Yb, 10/10.21$^{@}$ *-12.61*	111YAG Air	$CaCO_3$ 2.5N Nb_2O_5 3N,Yb_2O_3 4.8N	1.8(N+Sh) 2(B+T)	20(S+Sh+B) 15(T)	21.65-9 → 60 9-2 → 30		0.0136	Y	22.1	15.22	487±8	65-65 / 99-99 / 87-74
Yb, 11.6/12.07$^{@}$ -14.99	Pt Air	$CaCO_3$ 2.5N Nb_2O_5 3N, Yb_2O_3 3N	1.1	20	22.66-19 → 48 19-11-3 → 48-48	1932.01		LY	13.6	1.12	406±15	54-33 / 245-234 / 97-86 50-42 /158-180 / 81-70
Yb, 15/18.86$^{@}$ -23.40	Pt Air	$CaCO_3$ 2.5N Nb_2O_5 3N, Yb_2O_3 3N	2	20	21.22-10 → 30 10-2 → 20h	1934.57		Y	8.57	1.95	275±18	NO LASING
Na-modified Yb:CNNGG												
Na, 3/0.84$^{@}$ Yb, 3/1.74$^{@}$	Pt Air	Ca/Na_2CO_3 2.5N Nb_2O_5 3N, Yb_2O_3 4N	1.4(N) 1.9(Sh+B+T)	20	21.3-10 → 50 10-0 → 20		0.02846	G	178	6.29	647	49-46 / 134-134 / 81-76
Na, 5.8/0.93$^{@}$ Yb, 5.8/7.96$^{@}$	Pt Air	Ca/Na_2CO_3 2.5N Nb_2O_5 3N, Yb_2O_3 4N	1.4(N) 1.65(Sh) 1.9(B+T)	30(S+Sh) 25(B); 20(T)	22.47-12 → 48 12-3 → 48			GY	35.3	7.58	578±10	74-73 / 98-86 / 85-74
Na, 12/6.17$^{@}$ Yb, 6/5.87$^{\#}$	111YAG Air	Ca/Na_2CO_3 2.5N Nb_2O_5 3N, Yb_2O_3 4N	1.5(N);1.8(Sh) 2(B+T)	30(S+Sh) 25(B);20(T)	22.47-12 → 48 12-3 → 48			G	129.7	11.5	579±30	51-51 / 90-90 / 74-61

Na, 6/2.55 Yb, 7/7.9[@]	111YAG Air	Ca/Na_2CO_3 2.5N Nb_2O_5 3N, Yb_2O_3 4N	1.8(N+Sh) 2(B+T)	20(S+Sh) 20(B); 15(T)	19.9-8 → 50 8-2→ 50			G	64.8	9.71	526±26	71-70 / 118-89 / 74-58
Na, 8/2.3[@] Yb, 8/9.6[@]	Pt Air	Ca/Na_2CO_3 2.5N Nb_2O_5 3N, Yb_2O_3 4N	1.4(N); 1.5(Sh) 1.7(B+T)	35(S+Sh+C) 30(B);25(T)	20.3-12 → 48 12-3 → 48		0.03439	GY	51.8	12.17	470±7	64-64 / 93-93 / 73-58
Na, 8/2.26[@],2.73* Yb, 8/8.77[@] *-10.78*	Pt Air	$CaCO_3$ 4N Na_2CO_3 4.7N Nb_2O_5 4N, Yb_2O_3 4N	1.2(N) 1.5(Sh) 1.7(B+T)	20	22-10 → 45 10-0 → 15		0.01593	Y	15.5	7.4		66-66 / 100-100 / 92-79
Na, 16/4.95[@]-11.8[+] Yb, 8/10.4[@] -12.81	Pt Air	Ca/Na_2CO_3 2.5N Nb_2O_5 3N, Yb_2O_3 4N	1.6(N) 1.8(Sh) 2.1(B+T)	30(S+Sh); 25 (B+T)	19.7-13 → 50 13-3 → 50	1947.97		Y	18.5	6.5	529±13	69-59 / 185-134 / 84-71
Na, 9.8/1.44[@] Yb, 8.4/10.54[@]	111YAG O_2	Ca/Na_2CO_3 2.5N Nb_2O_5 3N, Yb_2O_3 4N	1.6(N) 1.8(Sh) 2.1(B+T)	30(S+Sh); 25 (B+T)	20.5-13 → 50 13-0 → 50		0.01363	Y	43.3	12.24	490±10	58-50 / 115-115 / 81-64
Na, 9.1/-- Yb, 8.7/9.34[#]	Pt O_2	Ca/Na_2CO_3 2.5N Nb_2O_5 3N, Yb_2O_3 3N+4N	2	20	22.6-10 → 45 10-2 → 15		0.05312	Y	30.86	16.8		39-32 /295-245 / 96-89
Na, 6.5/1.5[@] Yb, 10/12.6[@]	111YAG Air	Ca/Na_2CO_3 2.5N Nb_2O_5 3N, Yb_2O_3 4.8N	1.3(N);1.6(Sh) 1.8(B+T)	20(S+Sh+B) 18 (B) 15 (T)	20.4-2 → 90		0.01287	Y	26.9	13.92	391±12	62-62 / 107-107 / 81-68
Na, 10/2.86[@]-6.2[+] Yb, 10/13.2-12.6[@]-15.86	111YAG Air	Ca/Na_2CO_3 2.5N Nb_2O_5 3N, Yb_2O_3 4.N	1.5(N) 1.8(Sh) 2.0(B+T)	20(S+Sh+B) 18 (B) 15 (T)	20.4-8 → 35 8-2 →10	1935.27		Y	30.1	16.4	432±13	54- ? / 177- ? / 84-75
Na, 12/3.7[@]-3.82*-5.6[+] Yb, 12/14.67[@]-18.159	Pt Air	Ca/Na_2CO_3 2.5N Nb_2O_5 3N, Yb_2O_3 4N	1.2(N) 1.4(Sh) 1.7(B+T)	15	21.05-18 → 50 18-3 → 90	1934.95		Y	19.4	9.58	406±24	66-66 / 92-92 / 75-62
Na, 30/12.23*-13.8 [+]Yb, 5/7.13[@]-8.78	Pt Air	Ca/Na_2CO_3 2.5N Nb_2O_5 3N, Yb_2O_3 4N	1.8	20	15.5-8 → 40 10-2 → 10	1947.65					568	68-65 / 69-52 / 61-54
Li-modified Yb:CLNGG												
Yb, 0		Ca/$^6Li_2CO_3$ 2.5N/1.5	2	20	21.81-10 → 50 10-2 → 90	1956.13	0.00786	Y	22.68	5.69		
Yb, 8/7.57[@]-9.34	Pt Air	Ca/ Li_2CO_3 2.5N/2N Nb_2O_5 4N, Yb_2O_3 4N	1.8	20	23.11-10 → 40 10-2 → 10	1944.93	0.00786	Y	18.6	6.54	541	85-80 / 75-78 / 74-60
Yb, 8/7.28[#]	Pt Air	Ca/Li_2CO_3 4N/4.7N Nb_2O_5 4N, Yb_2O_3 4N	1.3(N) 1.8(Sh+B+T)	20	22.55-10 → 50 10-0 →20		0.01711	LY	5.37	0.68		72-69 / 68-50 / 72-67
Li & Na-modified Yb:CLNNGG												
Na, 30/6.09[@] Yb, 8/9.35[@]	Pt Air	$CaCO_3$ 4N/ Li_2/Na_2CO_3 4.7N Yb_2O_3 4N	1.2(N) 1.5(Sh) 1.65(B+T)	20	18.3-10 → 60 10-0 → 20			CL	0.56	1		71-66 / 120-115 / 87-73
Na, 30/12.56* Yb, 8/9.45[#]	Pt Air	$CaCO_3$ 4N Li/Na_2CO_3 4.7N Yb_2O_3 4N	1.7	20	18.6-10 → 75 10-0 → 40			LY	6	0.85		73-69 / 165-160 / 96-93

v) Crystallographic information

Crystal structures were determined from scXRD data collected at 300 K in a Bruker Kappa Apex II diffractometer equipped with a fine-focus sealed tube working at 50 kV/30 mA. Mo K_α radiation (0.71073 Å) was selected with a graphite monochromator. Table ESI.4 provides the crystal data and structure refinement details for each of the analyzed crystals. The collected frames were integrated with the Bruker SAINT software package using a narrow-frame algorithm. Using cubic unit cells, the total number of reflections yielded by the integration of the data up to the corresponding maximum measured θ angle have been also included in Table ESI.4. The starting unit cell constants were determined from the refinement of the XYZ-centroids of a given number of reflections with intensity above 20 σ(I). Data were corrected for absorption using the multi-scan method (SADABS). All calculations were performed using the SHELXTL program. Atomic coordinates *x, y, z* (x 10^4), occupancy factors OF and equivalent isotropic displacement parameters U(eq) (Å^{2}x 10^3) are given in Table ESI.5. Bond lengths (Å) are given in Table ESI.6 and Table ESI.7 gives the corresponding anisotropic displacement parameters.

The structure parameters were refined in several steps. The relative populations of Ca^{2+}, Ca^{2+}/Yb^{3+} or $Ca^{2+}/Yb^{3+}/Na^{+}$ in dodecahedral {24*c*} sites, and Ga^{3+}/Nb^{5+} over both octahedral [16*a*] and tetrahedral (24*d*) garnet sites were primarily estimated from successive refinements carried out with starting data from the CNGG proposed structure model, [2] in which positional and isotropic displacement parameters were also refined but oxygen occupancy factor (OF) was fixed. These initial refinements indicate that while octahedral sites are fully occupied by Nb^{5+} and Ga^{3+} in a ratio of ≈2:1 (the presence of Ca^{2+} was discarded), vacancies over dodecahedral and tetrahedral sites may be present. Then, for each crystal the cationic OF over the three sites and anisotropic displacement parameters for all atoms were simultaneously refined, while the oxygen OF was still kept fixed. The refinements yielded positive values of the anisotropic displacement parameters for all atoms in these crystals, with very low R_1 [I>2σ(I)] discrepancy factors. Finally the oxygen OF was also refined along with all cationic OF and anisotropic displacement parameters. From this final refinement the full occupancy of the 96*h* oxygen site is established for all analyzed crystals.

Table ESI.4. 300 K crystal data and structure refinement details of Yb:CNGG-type garnets. X-ray wavelength λ= 0.71073 Å. Cubic crystal system with *Ia*-3*d* (230) space group, Z= 8.

Dopants in the melt (at %)	Undoped	11.6 Yb	10 Na:10 Yb	12 Na:12 Yb	16 Na:8 Yb	30 Na:8 Yb
Unit cell dimension *a* (Å)	12.4969(1)	12.4548(3)	12.4618(2)	12.4611(1)	12.4842(1)	12.4883(1)
Volume ($Å^3$)	1951.67(3)	1932.01(8)	1935.27(5)	1934.95(3)	1945.73(3)	1947.65(3)
Density (Mg/m^3)	4.814	4.966	4.780	5.158	4.878	4.178
Absorption coefficient (mm^{-1})	12.000	16.129	14.787	17.112	14.395	10.837
Crystal size (mm^3)	0.070x0.120x0.210	0.001x0.046x0.067	0.001x0.032x0.089	0.050x0.130x0.180	0.07x0.080x0.190	0.025x0.052x0.075
Collection θ range (deg)	3.99 to 28.30	4.01 to 30.37	4.01 to 36.45	4.01 to 30.35	4.00 to 30.61	4.00 to 30.49
Index ranges, *h* *k* *l*	-16 to 16 -16 to 16 -16 to 16	-16 to 17 -17 to 17 -17 to 17	-17 to 20 -12 to 20 -20 to 20	-17 to 17 -17 to 16 -17 to 17	-17 to 16 -16 to 17 -17 to 17	-17 to 17 -17 to 17 -17 to 17
Reflections collected	52659	14476	9127	17155	20160	67426
Independent reflections R (int)	211 0.0426	251 0.0626	404 0.0898	250 0.0438	255 0.0484	254 0.0518
Completeness to θ (deg) (%)	28.30 100.0	30.37 100.0	36.45 100.0	30.35 99.6%	30.61 100.0	30.49 100.0
Absorption correction	SADABS					
Refinement method	Full-matrix least squares on F^2					
Goodness-of-fit on F^2	1.354	1.080	1.030	1.171	1.154	1.399
R indices [I>2σ(I)], R_1 wR_2	0.0109 0.0310	0.0125 0.0189	0.0236 0.0369	0.0129 0.0295	0.0127 0.0260	0.0103 0.0168
R indices (all data), R_1 wR_2	0.0121 0.0335	0.0304 0.0223	0.0641 0.0497	0.0164 0.0316	0.0160 0.0282	0.0173 0.0219
Extinction coefficient	0.00124(8)	0.00008(2)	0.00031(5)	0.00118(8)	0.00280(10)	0.00059(3)
Largest diff. peak and hole ($e.Å^{-3}$)	0.279 and -0.321	0.331 and -0.428	0.638 and -0.840	0.339 and -0.380	0.274 and -0.293	0.280 and -0.411

Table ESI.5. Atomic coordinates *x, y, z* (x10^4), occupancy factors OF and equivalent isotropic displacement parameters U(eq) (Å^{2}x10^3) for Yb:CNGG and Yb:CNNGG crystals. U(eq) es 1/3 of the trace of the orthogonalized U^{ij} tensor. Dopant concentrations (at%) are in the melt.

Undoped CNGG, $\{Ca_{2.96}\Diamond_{0.04}\}[Nb_{1.25}Ga_{0.75}](Ga_{2.5}Nb_{0.3¤0.2})$

Atom	site	*x*	*y*	*z*	OF	U(eq)
Ca	24*c*	0	2500	11250	0.987(6)	11(1)
Nb1	16*a*	0	5000	10000	0.623(4)	5(1)
Ga1	16*a*	0	5000	10000	0.374(4)	5(1)
Ga2	24*d*	0	2500	8750	0.82(4)	7(1)
Nb2	24*d*	0	2500	8750	0.10(4)	7(1)
O	96*h*	504(1)	1476(1)	9693(1)	0.994(8)	10(1)

11.6 at%Yb:CNGG, $\{Ca_{2.60}Yb_{0.31}\Diamond_{0.09}\}[Nb_{1.26}Ga_{0.68}](Ga_{2.77}Nb_{0.01¤0.23})$

Atom	site	*x*	*y*	*z*	OF	U(eq)
Ca	24*c*	10000	2500	1250	0.868(2)	10(1)
Yb	24*c*	10000	2500	1250	0.102(2)	10(1)
Nb1	16*a*	10000	5000	0	0.63(4)	5(1)
Ga1	16*a*	10000	5000	0	0.34(4)	5(1)
Ga2	24*d*	10000	2500	3750	0.922(4)	7(1)
Nb2	24*d*	10000	2500	3750	0.003(4)	7(1)
O	96*h*	9696(1)	510(1)	1483(1)	0.999(6)	10(1)

10 at% Na: 10 at% Yb:CNNGG, $\{Ca_{2.35}Yb_{0.35}Na_{0.18}\Diamond_{0.12}\}[Nb_{1.32}Ga_{0.68}](Ga_{2.75}Nb_{0.07¤0.18})$

Atom	site	*x*	*y*	*z*	OF	U(eq)
Ca	24*c*	10000	2500	1250	0.783(4)	9(1)
Yb	24*c*	10000	2500	1250	0.117(2)	9(1)
Na	16*a*	10000	2500	1250	0.059(4)	9(1)
Nb1	16*a*	10000	5000	0	0.659(4)	5(1)
Ga1	24*d*	10000	5000	0	0.341(4)	5(1)
Ga2	24*d*	10000	2500	3750	0.918(4)	8(1)
Nb2	96*h*	10000	2500	3750	0.022(4)	8(1)
O	24*c*	9697(2)	509(2)	1482(2)	1.01(1)	11(1)

12 at%Na:12 at%Yb:CNNGG, $\{Ca_{2.35}Yb_{0.48}Na_{0.17}\}[Nb_{1.55}Ga_{0.45}](Ga_{2.82}Nb_{0.06¤0.12})$

Atom	site	*x*	*y*	*z*	OF	U(eq)
Ca	24*c*	1250	0	2500	0.783(4)	10(1)
Yb	24*c*	1250	0	2500	0.161(2)	10(1)
Na	24*c*	1250	0	2500	0.056(4)	10(1)
Nb1	16*a*	0	0	0	0.773(4)	5(1)
Ga1	16*a*	0	0	0	0.227(4)	5(1)
Ga2	24*d*	-1250	0	2500	0.94(4)	7(1)
Nb2	24*d*	-1250	0	2500	0.02(4)	7(1)
O	96*h*	-302(1)	515(1)	1483(1)	0.993(8)	9(1)

16 at%Na:8 at%Yb:CNNGG, $\{Ca_{2.37}Yb_{0.28}Na_{0.35}\}[Nb_{1.32}Ga_{0.68}](Ga_{2.79}Nb_{0.03¤0.18})$

Atom	site	*x*	*y*	*z*	OF	U(eq)
Ca	24*c*	1250	0	2500	0.791(4)	10(1)
Yb	24*c*	1250	0	2500	0.093(1)	10(1)
Na	24*c*	1250	0	2500	0.116(4)	10(1)
Nb1	16*a*	0	0	0	0.661(4)	5(1)
Ga1	16*a*	0	0	0	0.339(4)	5(1)
Ga2	24*d*	-1250	0	2500	0.93(4)	7(1)
Nb2	24*d*	-1250	0	2500	0.01(4)	7(1)
O	96*h*	-305(1)	509(1)	1479(1)	0.999(7)	11(1)

30 at%Na:8 at%Yb:CNNGG, $\{Ca_{2.44}Yb_{0.15}Na_{0.41}\}[Nb_{1.10}Ga_{0.90}](Ga_{2.48}Nb_{0.26¤0.27})$

Atom	site	*x*	*y*	*z*	OF	U(eq)
Ca	24*c*	10000	2500	1250	0.814(4)	9(1)
Yb	24*c*	10000	2500	1250	0.051(1)	9(1)
Na	16*a*	10000	2500	1250	0.135(4)	9(1)
Nb1	16*a*	10000	5000	0	0.550(4)	4(1)
Ga1	24*d*	10000	5000	0	0.450(4)	4(1)
Ga2	24*d*	10000	2500	3750	0.825(4)	7(1)
Nb2	96*h*	10000	2500	3750	0.085(4)	7(1)
O	24*c*	9693(1)	503(1)	1476(1)	0.999(6)	11(1)

Table ESI.6. Bond lengths (Å) for undoped CNGG, YbCNGG and Yb:CNNGG. Dopant concentrations are in the melt.

Undoped[a]		11.6 at%Yb:CNGG[b]		10at%Na:10at%Yb:CNNGG[c]		12at%Na:12at%Yb:CNNGG[d]		16 at% Na:8 at% Yb[e]		30at%Na:8at%Yb:CNNGG[f]	
Ca-O1#1	2.4126(12)	Ca-O1#1	2.3989(15)	Ca-O#1	2.399(2)	Ca-O#1	2.3994(13)	Ca-O1	2.4075(12)	Ca-O#1	2.4103(13)
Ca-O1#2	2.4126(12)	Ca-O1#2	2.3989(15)	Ca-O#2	2.399(2)	Ca-O	2.3994(13)	Ca-O1#1	2.4075(12)	Ca-O#2	2.4103(13)
Ca-O1	2.4126(12)	Ca-O1#3	2.3989(15)	Ca-O#3	2.399(2)	Ca-O#2	2.3994(13)	Ca-O1#2	2.4075(12)	Ca-O#3	2.4103(13)
Ca-O1#3	2.4126(12)	Ca-O1#4	2.3989(15)	Ca-O#4	2.399(2)	Ca-O#3	2.3994(13)	Ca-O1#3	2.4075(12)	Ca-O#4	2.4103(13)
Ca-O1#4	2.5391(13)	Ca-O1#5	2.5240(16)	Ca-O#5	2.527(2)	Ca-O#4	2.5192(13)	Ca-O1#4	2.5313(12)	Ca-O#5	2.5387(14)
Ca-O1#5	2.5391(13)	Ca-O1#6	2.5240(16)	Ca-O	2.527(2)	Ca-O#5	2.5192(13)	Ca-O1#5	2.5313(12)	Ca-O	2.5387(14)
Ca-O1#6	2.5391(13)	Ca-O1#7	2.5240(16)	Ca-O#6	2.527(2)	Ca-O#6	2.5192(13)	Ca-O1#6	2.5313(12)	Ca-O#6	2.5387(14)
Ca-O1#7	2.5391(13)	Ca-O1	2.5240(16)	Ca-O#7	2.527(2)	Ca-O#7	2.5192(13)	Ca-O1#7	2.5313(12)	Ca-O#7	2.5387(14)
Ca-Ga2	3.1242	Ca-Ga2	3.1137	Ca-Ga2	3.1154	Ca-Ga2	3.1153	Ca-Ga2	3.1211	Ca-Ga2	3.1221
Ca-Nb2#8	3.1242	Ca-Nb2#8	3.1137	Ca-Nb2#8	3.1154	Ca-Nb2#8	3.1153	Ca-Nb2#8	3.1211	Ca-Nb2#8	3.1221
Ca-Ga2#8	3.1242	Ca-Ga2#8	3.1137	Ca-Ga2#8	3.1154	Ca-Ga2#8	3.1153	Ca-Ga2#8	3.1211	Ca-Ga2#8	3.1221
Nb1-O1#3	1.9864(12)	Nb1-O1#3	1.9894(15)	Nb1-O#4	1.988(2)	Nb1-O#7	1.9918(12)	Nb1-O1#7	1.9897(11)	Nb1-O#4	1.9854(13)
Nb1-O1#7	1.9864(12)	Nb1-O1#9	1.9894(15)	Nb1-O#7	1.988(2)	Nb1-O#9	1.9918(12)	Nb1-O1	1.9897(11)	Nb1-O#9	1.9854(13)
Nb1-O1#9	1.9864(12)	Nb1-O1#10	1.9894(15)	Nb1-O#9	1.988(2)	Nb1-O	1.9918(12)	Nb1-O1#9	1.9897(11)	Nb1-O#7	1.9854(13)
Nb1-O1#10	1.9864(12)	Nb1-O1#11	1.9894(15)	Nb1-O#10	1.988(2)	Nb1-O#10	1.9918(12)	Nb1-O1#10	1.9897(11)	Nb1-O#10	1.9854(13)
Nb1-O1#11	1.9864(12)	Nb1-O1#6	1.9894(15)	Nb1-O#11	1.988(2)	Nb1-O#11	1.9918(12)	Nb1-O1#11	1.9897(11)	Nb1-O#11	1.9854(13)
Nb1-O1#12	1.9864(12)	Nb1-O1#12	1.9894(15)	Nb1-O#12	1.988(2)	Nb1-O#12	1.9918(12)	Nb1-O1#12	1.9897(11)	Nb1-O#12	1.9854(13)
Nb1-Ca#13	3.4930	Nb1-Ca#13	3.4812	Nb1-Na#13	3.4832	Nb1-Ca#12	3.4830	Nb1-Ca#12	3.4894	Nb1-Na#13	3.4906
Nb1-Ca#14	3.4930	Nb1-Yb#13	3.4812	Nb1-Ca#13	3.4832	Nb1-Ca#11	3.4830	Nb1-Ca#10	3.4894	Nb1-Ca#13	3.4906
Nb1-Ca#7	3.4930	Nb1-Ca#14	3.4812	Nb1-Yb#13	3.4832	Nb1-Ca#10	3.4830	Nb1-Ca#9	3.4894	Nb1-Yb#13	3.4906
Nb1-Ca#10	3.4930	Nb1-Yb#1	3.4812	Nb1-Na#14	3.4832	Nb1-Yb#9	3.4830	Nb1-Yb#11	3.4894	Nb1-Na#14	3.4906
Nb1-Ca#15	3.4930	Nb1-Yb#15	3.4812	Nb1-Ca#14	3.4832	Nb1-Yb#7	3.4830	Nb1-Yb#7	3.4894	Nb1-Ca#14	3.4906
Ga2-O1#16	1.8505(13)	Ga2-O1#16	1.8429(15)	Nb1-Yb#14	3.4832	Ga2-O#13	1.8476(13)	Ga2-O1#13	1.8490(12)	Nb1-Yb#14	3.4906
Ga2-O1#3	1.8505(13)	Ga2-O1#4	1.8429(15)	Ga2-O#15	1.845(2)	Ga2-O#3	1.8476(13)	Ga2-O1#3	1.8489(12)	Ga2-O#15	1.8482(13)
Ga2-O1	1.8505(13)	Ga2-O1#17	1.8429(15)	Ga2-O#16	1.845(2)	Ga2-O#14	1.8476(13)	Ga2-O1#14	1.8489(12)	Ga2-O#16	1.8482(13)
Ga2-O1#17	1.8505(13)	Ga2-O1#2	1.8429(15)	Ga2-O#2	1.845(2)	Ga2-O	1.8476(13)	Ga2 -O1	1.8490(12)	Ga2-O#2	1.8482(13)
Ga2-Ca#18	3.1242	Ga2-Yb#18	3.1137	Ga2-O#3	1.845(2)	Ga2-Ca#15	3.1153	Ga2-Ca#15	3.1210	Ga2-O#3	1.8482(13)
O1-Ga1#3	1.9864(12)	Ga2-Ca#18	3.1137	Ga2-Yb#17	3.1154	Ga2-Yb#15	3.1153	Ga2-Yb#15	3.1210	Ga2-Yb#17	3.1221
O1-Nb1#3	1.9864(12)	O1-Nb2#19	1.8429(15)	Ga2-Na#17	3.1154	Ga2-Na#15	3.1153	Ga2-Na#15	3.1210	Ga2-Na#17	3.1221
O1-Ca#19	2.5391(13)	O1-Ga2#19	1.8429(15)	Ga2-Ca#17	3.1154	O-Na#11	2.5192(13)	O1-Na#10	2.5313(12)	Ga2-Ca#17	3.1221
		O1-Ga1#6	1.9894(15)	O-Nb2#18	1.845(2)	O-Ca#11	2.5192(13)	O1-Ca#10	2.5313(12)	O-Nb2#18	1.8482(13)
		O1-Nb1#6	1.9894(15)	O-Ga2#18	1.845(2)	O-Yb#11	2.5192(13)	O1-Yb#10	2.5313(12)	O-Ga2#18	1.8482(13)
		O1-Ca#20	2.3989(15)	O-Ga1#7	1.988(2)					O-Ga1#7	1.9854(13)
		O1-Yb#20	2.3989(15)	O-Nb1#7	1.988(2)					O-Nb1#7	1.9854(13)
				O-Ca#19	2.399(2)					O-Ca#19	2.4103(13)
				O-Yb#19	2.399(2)					O-Yb#19	2.4103(13)
				O-Na#19	2.399(2)					O-Na#19	2.4103(13)

[a] Symmetry transformations used to generate equivalent atoms:

#1 -y+1/4,-x+1/4,-z+9/4 #2 y-1/4,x+1/4,-z+9/4

#3 -x+0,-y+1/2,z+0 #4 z-1,x,y+1 #5 -x+1/4,-z+5/4,-y+5/4

#6 x-1/4,z-3/4,-y+5/4 #7 -z+1,-x+1/2,y+1 #8 x,-y+1/2,z+1/2

#9 y,z-1/2,-x+1 #10 z-1,x+1/2,-y+1 #11 x,y+1/2,-z+2

#12 -y+0,-z+3/2,x+1 #13 y-1/2,-z+3/2,-x+1 #14 -y+1/2,z-1/2,x+1

#15 -x,-y+1,-z+2 #16 y-1/4,-x+1/4,-z+7/4 #17 -y+1/4,x+1/4,-z+7/4

#18 x,-y+1/2,z-1/2 #19 y,z-1,x+1

[b] Symmetry transformations used to generate equivalent atoms:

#1 y+1,z,x-1 #2 -z+5/4,-y+1/4,-x+5/4 #3 -y+1,-z+1/2,x-1

#4 z+3/4,y+1/4,-x+5/4 #5 y+3/4,x-3/4,-z+1/4

#6 -x+2,-y+1/2,z+0 #7 -y+5/4,-x+5/4,-z+1/4 #8 x,-y+1/2,z-1/2

#9 y+1,z+1/2,-x+1 #10 z+1,x-1/2,-y #11 -z+1,-x+3/2,y+0

#12 x,y+1/2,-z #13 y+1/2,-z+1/2,-x+1 #14 -y+3/2,z+1/2,x-1

#15 -x+2,-y+1,-z #16 y+1,-z+1/2,x-1/2 #17 -y+1,z,x-1/2

#18 x,-y+1/2,z+1/2 #19 z+1/2,x-1,-y+1/2 #20 z+1,x-1,y

[c] Symmetry transformations used to generate equivalent atoms:

#1 y+1,z,x-1 #2 -z+5/4,-y+1/4,-x+5/4 #3 z+3/4,y+1/4,-x+5/4

#4 -y+1,-z+1/2,x-1 #5 y+3/4,x-3/4,-z+1/4 #6 -y+5/4,-x+5/4,-z+1/4

#7 -x+2,-y+1/2,z+0 #8 x,-y+1/2,z-1/2 #9 z+1,x-1/2,-y

#10 y+1,z+1/2,-x+1 #11 x,y+1/2,-z #12 -z+1,-x+3/2,y+0

#13 y+1/2,-z+1/2,-x+1 #14 -y+3/2,z+1/2,x-1 #15 -y+1,z,x-1/2

#16 y+1,-z+1/2,x-1/2 #17 x,-y+1/2,z+1/2 #18 z+1/2,x-1,-y+1/2

#19 z+1,x-1,y

[d] Symmetry transformations used to generate equivalent atoms:

#1 -x+1/4,-z+1/4,-y+1/4 #2 -x+1/4,z-1/4,y+1/4

#3 x+0,-y+0,-z+1/2 #4 -z+1/4,y-1/4,x+1/4 #5 z+0,-x+0,-y+1/2

#6 -z+1/4,-y+1/4,-x+1/4 #7 z,x,y #8 x+1/2,y,-z+1/2

#9 -x,-y,-z #10 -y,-z,-x #11 y,z,x #12 -z,-x,-y

#13 -x-1/4,z-1/4,-y+1/4 #14 -x-1/4,-z+1/4,y+1/4

#15 x-1/2,y,-z+1/2

[e] Symmetry transformations used to generate equivalent atoms:

#1 -x+1/4,-z+1/4,-y+1/4 #2 -x+1/4,z-1/4,y+1/4

#3 x+0,-y+0,-z+1/2 #4 -z+1/4,y-1/4,x+1/4 #5 z+0,-x+0,-y+1/2

#6 -z+1/4,-y+1/4,-x+1/4 #7 z,x,y #8 x+1/2,y,-z+1/2

#9 -y,-z,-x #10 y,z,x #11 -x,-y,-z #12 -z,-x,-y

#13 -x-1/4,z-1/4,-y+1/4 #14 -x-1/4,-z+1/4,y+1/4

#15 x-1/2,y,-z+1/2

[f] Symmetry transformations used to generate equivalent atoms:

#1 y+1,z,x-1 #2 -z+5/4,-y+1/4,-x+5/4 #3 z+3/4,y+1/4,-x+5/4

#4 -y+1,-z+1/2,x-1 #5 -y+5/4,-x+5/4,-z+1/4 #6 y+3/4,x-3/4,-z+1/4

#7 -x+2,-y+1/2,z+0 #8 x,-y+1/2,z-1/2 #9 y+1,z+1/2,-x+1

#10 z+1,x-1/2,-y #11 x,y+1/2,-z #12 -z+1,-x+3/2,y+0

#13 y+1/2,-z+1/2,-x+1 #14 -y+3/2,z+1/2,x-1 #15 y+1,-z+1/2,x-1/2

#16 -y+1,z,x-1/2 #17 x,-y+1/2,z+1/2 #18 z+1/2,x-1,-y+1/2

#19 z+1,x-1,y

Table ESI.7. Anisotropic displacement parameters ($Å^2x10^3$) for undoped CNGG, Yb:CNGG and Yb:CNNGG garnets. Dopant concentrations are in the melt. The anisotropic displacement factor takes the form $-2\pi^2[h^2 a^{*2}U^{11} + ... + 2 h k a^* b^* U^{12}]$.

Undoped CNGG						
	U^{11}	U^{22}	U^{33}	U^{23}	U^{13}	U^{12}
Ca	13(1)	13(1)	7(1)	0	0	2(1)
Nb(1)	5(1)	5(1)	5(1)	0(1)	0(1)	0(1)
Ga(1)	5(1)	5(1)	5(1)	0(1)	0(1)	0(1)
Ga(2)	8(1)	8(1)	5(1)	0	0	0
Nb(2)	8(1)	8(1)	5(1)	0	0	0
O(1)	12(1)	8(1)	10(1)	1(1)	0(1)	0(1)

11.6 at% Yb:CNGG						
	U^{11}	U^{22}	U^{33}	U^{23}	U^{13}	U^{12}
Ca	11(1)	11(1)	6(1)	0	0	2(1)
Yb	11(1)	11(1)	6(1)	0	0	2(1)
Nb(1)	5(1)	5(1)	5(1)	0(1)	0(1)	0(1)
Ga(1)	5(1)	5(1)	5(1)	0(1)	0(1)	0(1)
Ga(2)	8(1)	8(1)	4(1)	0	0	0
Nb(2)	8(1)	8(1)	4(1)	0	0	0
O(1)	10(1)	13(1)	6(1)	0(1)	2(1)	0(1)

10 at% Na:10 at% Yb:CNNGG						
	U^{11}	U^{22}	U^{33}	U^{23}	U^{13}	U^{12}
Ca	11(1)	11(1)	5(1)	0	0	2(1)
Yb	11(1)	11(1)	5(1)	0	0	2(1)
Na	11(1)	11(1)	5(1)	0	0	2(1)
Nb(1)	5(1)	5(1)	5(1)	0(1)	0(1)	0(1)
Ga(1)	5(1)	5(1)	5(1)	0(1)	0(1)	0(1)
Ga(2)	9(1)	9(1)	6(1)	0	0	0
Nb(2)	9(1)	9(1)	6(1)	0	0	0
O	9(1)	16(1)	9(1)	1(1)	0(1)	1(1)

12 at% Na:12 at% Yb:CNNGG*						
	U^{11}	U^{22}	U^{33}	U^{23}	U^{13}	U^{12}
Ca	6(1)	12(1)	12(1)	2(1)	0	0
Yb	6(1)	12(1)	12(1)	2(1)	0	0
Na	6(1)	12(1)	12(1)	2(1)	0	0
Nb(1)	5(1)	5(1)	5(1)	0(1)	0(1)	0(1)
Ga(1)	5(1)	5(1)	5(1)	0(1)	0(1)	0(1)
Ga(2)	4(1)	8(1)	8(1)	0	0	0
Nb(2)	4(1)	8(1)	8(1)	0	0	0
O	9(1)	11(1)	7(1)	0(1)	1(1)	-1(1)

16 at% Na:8 at% Yb:CNNGG						
	U^{11}	**U^{22}**	**U^{33}**	**U^{23}**	**U^{13}**	**U^{12}**
Ca	6(1)	12(1)	12(1)	2(1)	0	0
Yb	6(1)	12(1)	12(1)	2(1)	0	0
Na	6(1)	12(1)	12(1)	2(1)	0	0
Nb(1)	5(1)	5(1)	5(1)	0(1)	0(1)	0(1)
Ga(1)	5(1)	5(1)	5(1)	0(1)	0(1)	0(1)
Ga(2)	5(1)	8(1)	8(1)	0	0	0
Nb(2)	5(1)	8(1)	8(1)	0	0	0
O(1)	11(1)	13(1)	8(1)	0(1)	1(1)	0(1)

30 at% Na:8 at% Yb:CNNGG						
	U^{11}	U^{22}	U^{33}	U^{23}	U^{13}	U^{12}
Ca	11(1)	11(1)	5(1)	0	0	2(1)
Yb	11(1)	11(1)	5(1)	0	0	2(1)
Na	11(1)	11(1)	5(1)	0	0	2(1)
Nb(1)	4(1)	4(1)	4(1)	0(1)	0(1)	0(1)
Ga(1)	4(1)	4(1)	4(1)	0(1)	0(1)	0(1)
Ga(2)	8(1)	8(1)	5(1)	0	0	0
Nb(2)	8(1)	8(1)	5(1)	0	0	0
O	11(1)	14(1)	8(1)	0(1)	1(1)	0(1)

vi) WDXRF analysis of Na

The Na content of three Yb:CNNGG and one Yb:CLNNGG crystals have been analyzed by Wavelength Dispersive X-ray Fluorescence (WDXRF). For this purpose specifically developed standards have been used and signal overlapping between Ga and Na X-ray emissions was accounted.

Five standards (crosses in Figure ESI.5) were prepared by mixing required amounts of $CaCO_3$, Na_2CO_3, Yb_2O_3, Nb_2O_5 and Ga_2O_3 precursor powders. After mixing and grinding twice, specific weights of these mixtures were melted in 5.50 g of anhydrous $Li_2B_4O_7$ (Merck) flux. A fully automated fusion machine (Perl´X3) and a 95%Pt+5%Au crucible were used for this purpose. This method produced glassy disks (32 mm of diameter and 3.8 mm of thickness) with known Na concentrations for analysis. Same sample preparation procedure was followed for the evaluation of the unknown Na content of the crystals, but in this case the crystals instead of precursor powders were grinded and weighted.

For elemental analyses a MagiX sequential WDXRF spectrometer equipped with a 2.4 kW generator and a Rh anode Super Sharp Tube with an ultrathin-window was used. The instrument optics is designed to allow a close coupling of the anode and the sample, resulting in excellent sensitivity. The irradiation spot on the sample has a diameter of 27 mm. The software for equipment control was the PANanalytical´s superQ which also incorporates items such as the generation of theoretical matrix correction coefficients, spectral overlap correction factors and drift corrections for quantitative composition analysis.

We first considered the interference between the Ga Lα,Lη (1.098, 0.984 keV) and Na Kα (1.041 keV) emissions. For this purpose the signal of a Na-free Yb:CNGG crystal (symbols in Figure ESI.6) was monitored and discounted from the signals of Yb:CNNGG ones (lines in Figure ESI.6). Figure ESI.6 (dashed line) also shows the difference found for the crystal with highest Yb content, which is representative of the Na concentration in this crystal. This procedure was applied both to the standards and to the crystals.

The analysis of the five standards (+) with Na concentrations ranging from 0 to 1.5 wt% provided the calibration line shown in Figure ESI.5. The Na concentration in the Yb:CNGG-type single crystals was determined by using this calibration line.

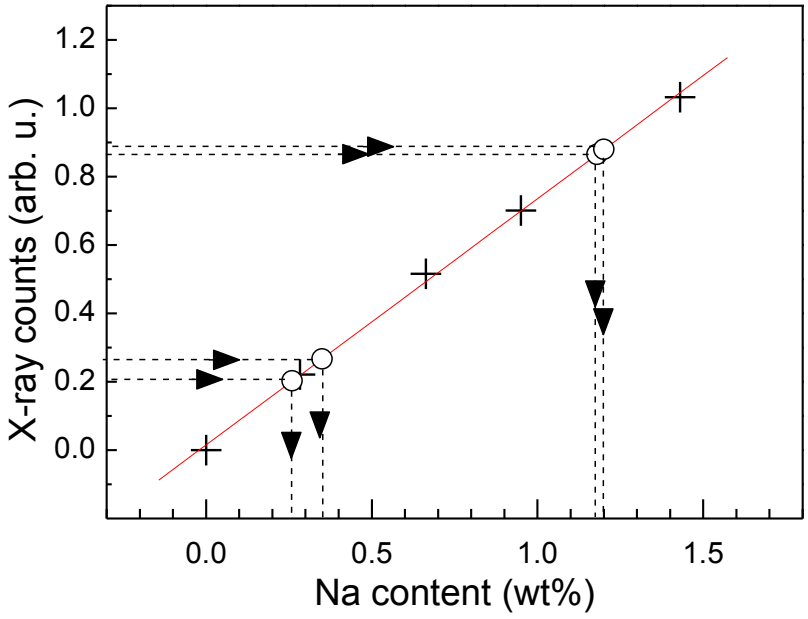

Figure ESI.5. WDXRF determination of Na concentration in Yb:CNGG-type crystals. The crosses are the results for standards with known Na concentration. The red line is the calibration obtained from the best fit of the standard results. The circles are for the crystals with unknown Na concentration.

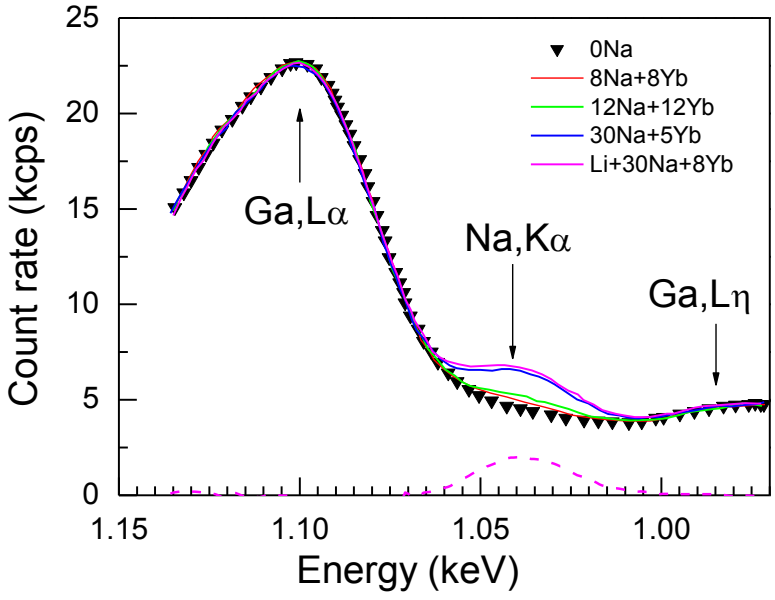

Figure ESI.6. Interference between Ga Lα, Lη and Na Kα X-ray emissions. Symbols stand for Na-free Yb:CNGG crystal. Lines are the signals obtained with Yb.CNNGG and Yb:CLNNGG crystals with increasing Na concentrations. The dashed line shows the difference between the Na-free crystal and the Yb:CLNNGG crystal with 30at% Na excess.

vii) Thermal annealing of CNGG-type crystals

It is well known that thermal annealing of some single crystals in oxygen-rich or –deficient atmospheres may modify the crystal colour usually creating broad optical absorptions bands. Examples of this behavior have been found for bismuth sillenites, [3] niobates, [4,5] titanyl phosphates, [6] and alkali molybdates,[7,8,9] among other oxides. To test the oxidation/reduction capability of the presently studied garnets we have conducted thermal annealing of the crystals in air and under vacuum.

Crystals with intense green or yellow colouration were oxidized by air annealing at 1340 ºC for 48 h. The annealing treatment recrystallizes the sample surfaces but bulk sample transparency is kept. To properly monitor changes in the Red-NIR and pre-edge OA bands for each crystal two different thicknesses were studied. After the treatment 50-100 µm of each face were removed by polishing before OA measurement. Figures ESI.7a and ESI.7b show the oxidation annealing OA results. Optical absorption coefficient found changes are always smaller than 1 cm^{-1}, i.e. very minor (note that we use a logarithmic scale for the y-axis representation), and they can be attributed to uncertainty in the spectral baseline correction.

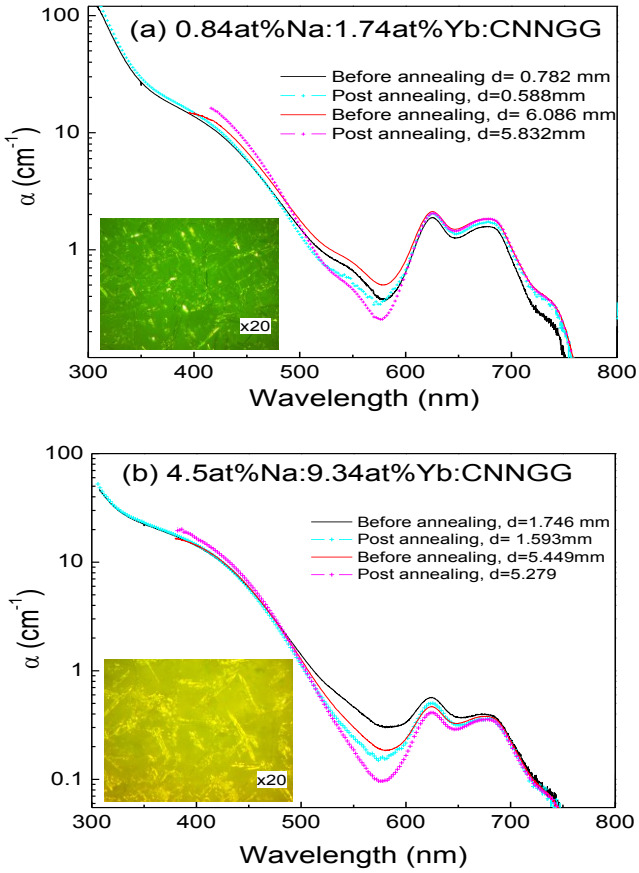

Figure ESI.7. 300 K optical absorption before and after 48 h of air annealing at 1340 ºC of Na-modified Yb:CNNGG crystals. a) 0.84at%Na:1.74at%Yb:CNNGG green crystal (Red-NIR $\int\alpha$= 178 cm^{-1}×nm, see Table ESI.3). b) 4.5at%Na:9.34at%Yb:CNNGG yellow crystal ($\alpha_{400\ nm}$= 16.8 cm^{-1}, see Table ESI.3) The insets show x20 magnified optical images of the corresponding unpolished crystal surfaces after oxidation.

Samples of a colourless ($\alpha_{400\ nm}$= 1 cm^{-1} and Red-NIR $\int\alpha$= 0.56 cm^{-1}×nm, see Table ESI.3) Li and Na modified CLNGG crystal were annealed inside a refractory steel tube in a 2.5x10^{-2} mbar of vacuum. The optical absorption spectra before and after consecutive 800 ºC and 900 ºC annealings are shown in Figure ESI.8. Apparently, a small increase of the pre-edge optical absorption is observed but it can not be straightforward assigned to oxygen deficiency because C and S contamination is evidenced by microprobe EDX studies, see Figure ESI.9. What is more remarkable in this study is the notable decrease of the surface Ga concentration induced by vacuum annealing and also of Yb although in a lesser extend. This is relevant for possible processing of this material as a transparent ceramic.

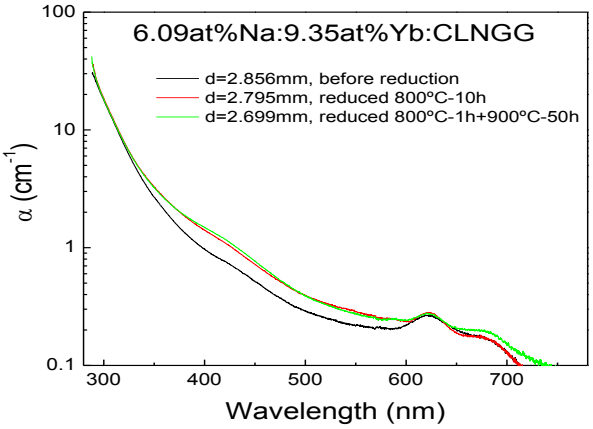

Figure ESI.8. 300 K OA changes induced by consecutive vacuum (2.5x10^{-2} mbar) annealing at 800 ºC/10h and 900ºC/48h of a Li and Na Yb:CLNNGG crystal.

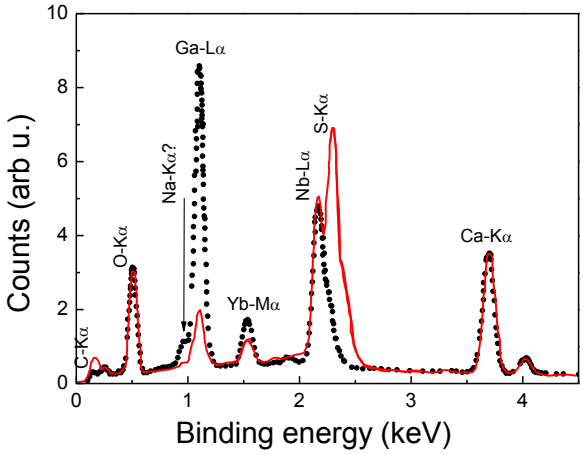

Figure ESI.9. Comparison of the composition of the Li and Na modified Yb:CLNGG crystal surface before (points) and after (red line) 800 ºC – 10 h vacuum (2.5x10^{-2} mbar) reduction. Note the Ga concentration decrease induced by the vacuum annealing. Observed C and S contamination is due to sublimation from the refractory steel tube used.

viii) Influence of Na on Yb^{3+} optical absorption cross section

Figure ESI.10 shows the evolution of the Yb^{3+} OA in Yb:CNNGG crystals with increasing Na content.

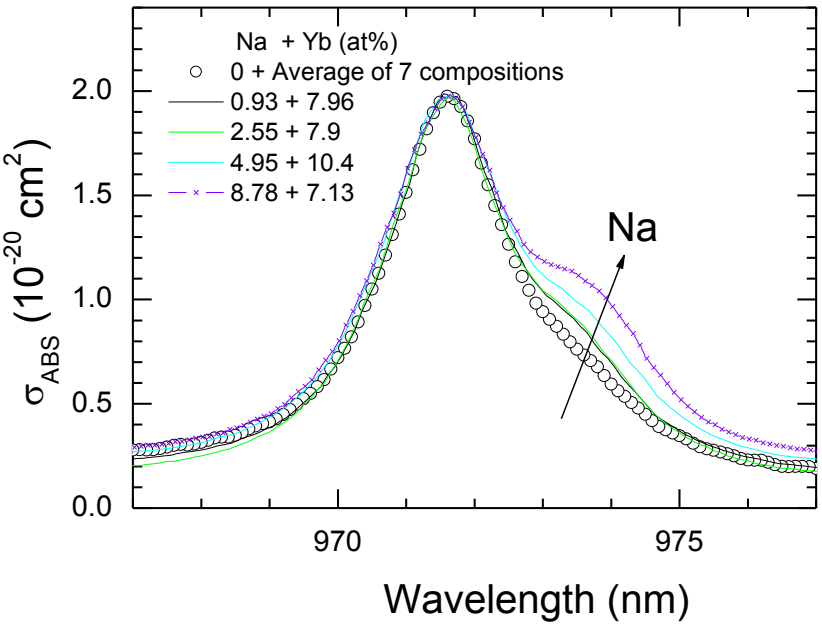

Figure ESI.10. Room temperature absorption cross section corresponding to the $^2F_{7/2}(0)\rightarrow{}^2F_{5/2}(0')$ Yb^{3+} transition as a function of increasing Na content in the Yb:CNNGG garnet crystal.

ix) Low temperature spectroscopy - Yb^{3+} energy levels

Low temperature (6 K) spectroscopy is commonly used to determine the level energies of trivalent lanthanides in solids, however, their determination for Yb^{3+} in the disordered CNGG-type single crystals is not a straightforward task because the Yb^{3+} center is not unique. This is clearly reflected in the shape and position of the Yb^{3+} $0\rightarrow0'$ transition shown in Figure ESI.10. It was already discussed in our previous work [¡Error! Marcador no definido.] that this band is mostly sensitive to the cationic electric charge of the two closest tetrahedra sharing edges with the Yb polyhedron but the occupancy of other Yb neighboring polyhedra plays also a role. Moreover, at low enough temperature only the ground $^2F_{7/2}(0)$ level is electronically populated, thus three optical absorption bands are expected to be observed from the crystal field splitting of the $^2F_{7/2}$ and $^2F_{5/2}$ Yb^{3+} multiplets. Contrary to this expectation at least four absorption bands are observed, the three at higher energy being strongly overlapped. The contribution of transitions starting at the excited $^2F_{7/2}(1)$ level is ruled out because such transitions (lying at the low energy side of the parent band) completely disappear at 6K for the $^2F_{7/2}(0)$ level, compare the shape of the OA spectra at 6K (Figure ESI.11) and 300 K (Figure 4a of the main text). Only two of the three bands observed at 922, 933 and 944 nm must correspond to direct $^2F_{7/2}(0)\rightarrow{}^2F_{5/2}(1',2')$ transitions of the majority Yb^{3+} center, the remaining one is more likely related either to the contribution of minority Yb^{3+}

centers or the result of coupling with a $\hbar\omega \approx 125$ cm^{-1} phonon. In order to include the whole energy range observed, for the partition functions calculations given in Section 3c of the main text we chosen E($^2F_{5/2}$)= 10299, 10593, 10850 cm^{-1} for the excited multiplet.

The energies of the Stark components of the ground $^2F_{7/2}$ multiplet were determined from 6K photoluminescence results, Figure ESI.12. Again the band-to-level assignment is not direct because the emission spectra are sensitive to the excitation wavelength, accordingly with the multisite character of the crystal. Nevertheless, these energies were established from the main features of the emission spectra as E($^2F_{7/2}$)= 0, 299, 518, 664 cm^{-1}. Figure ESI.13 sketches the energy levels and electronic transitions of an average Yb^{3+} centre in CNGG-type crystals. Note that although Na and Li modifications play indeed a role in the observed spectroscopy, for the energy level partition function calculation their influence has been ignored.

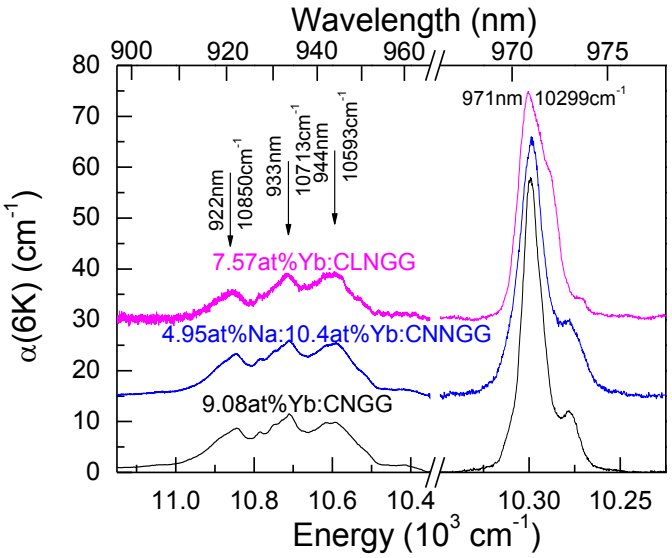

Figure ESI.11. 6K optical absorption of Yb doped CNGG-type single crystals.

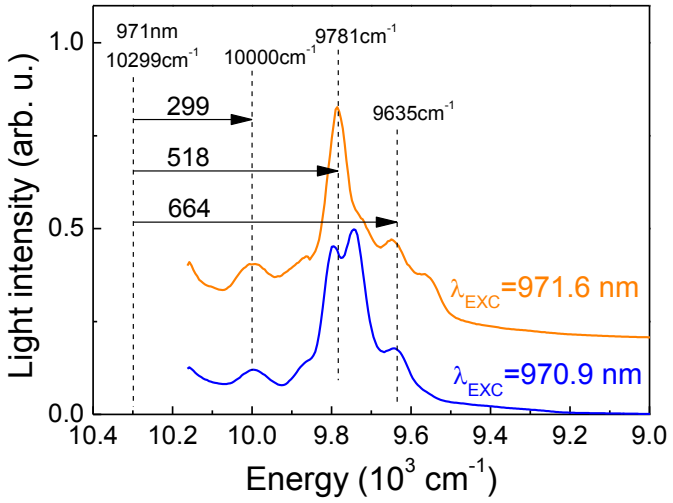

Figure ESI.12. 6K fluorescence of Yb doped CNGG single crystals.

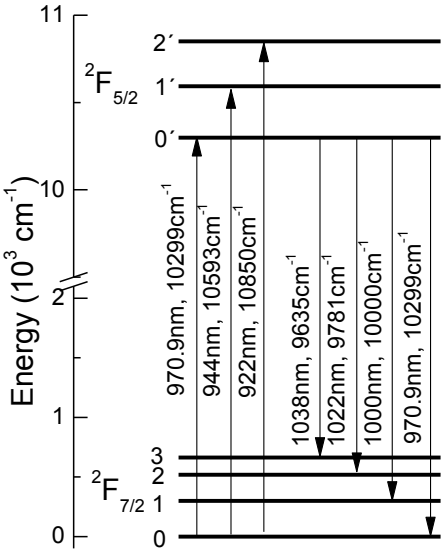

Figure ESI.13. Energy level and electronic transitions sketch for Yb^{3+} in CNGG-type crystals. E($^2F_{7/2}$)= 0, 299, 518, 664 cm^{-1}. E($^2F_{5/2}$)= 10299, 10593, 10850 cm^{-1}.

x) Yb^{3+} lifetime

The characterization of the Yb^{3+} lifetime (τ) in disordered crystals is a complex subject because of the coexistence of different Yb^{3+} centers, each potentially with different spectroscopic properties. In fact in a previous work [¡Error! Marcador no definido.] we have shown that the measured Yb^{3+} lifetime in CNGG depends on the excitation and emission wavelengths. Further, a common problem found in the values reported in the literature for Yb^{3+} is that they are enlarged by fluorescence reabsorption if specific care was not taken for their measurement. Basically this reabsorption can be circumvented or at least minimized either by using a very low Yb concentration or by testing a tiny sample volume near to the surface (crystal dispersion in liquids, very thin samples, <100 μm, or the pin hole method).

In our measurements we used a thin (60 μm) and low concentrated (0.08 at% Yb) CNGG crystal for the measurement of the radiative lifetime. For measurements in crystals with larger Yb concentration, these were ground and dispersed in ethilenglycol, the dispersion was diluted until the signal could be measured in the lowest scale of the oscilloscope and the result was averaged by 1000 acquisitions.

All luminescence decays obtained were well fit with a single exponential independently of temperature or Yb concentration tested. Figure ESI.14 shows the thermal evolution of the Yb^{3+} lifetime measured using a thin (60 μm) plate of a 0.08 at% Yb:CNGG. In it the Yb density is below 1×10^{19} at/cm^3, thus along with the low sample dimension fluorescence reabsorption can be fully ignored. τ slightly increases upon cooling reaching τ = 816 μs at 6K, which can be safely identified with the radiative lifetime for the dodecahedral Yb^{3+} in CNGG.

Figure ESI.15 shows that the 300 K Yb^{3+} lifetime decreases with increasing Yb concentration, this change is quite significant. At the maximum Yb concentration of 15 at%, still useful for laser purposes its value is reduced to half of the radiative value. Generally smaller values are found for crystals grown with 99.9% Yb_2O_3 than for those grown using 99.99% Yb_2O_3.

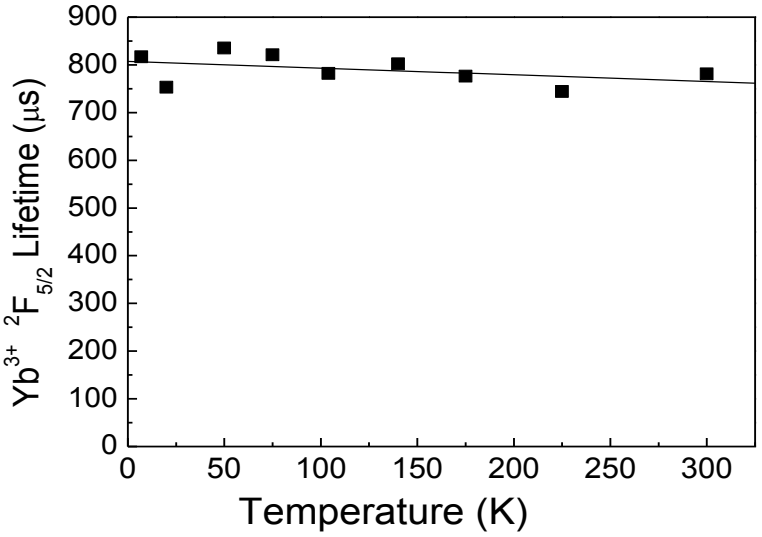

Figure ESI.14. Thermal evolution of the $^2F_{5/2}$ fluorescence lifetime of the dodecahedral Yb^{3+} center in the 0.08 at% Yb:CNGG crystal, λ_{EXC}= 971 nm, λ_{EMI}= 1021 nm.

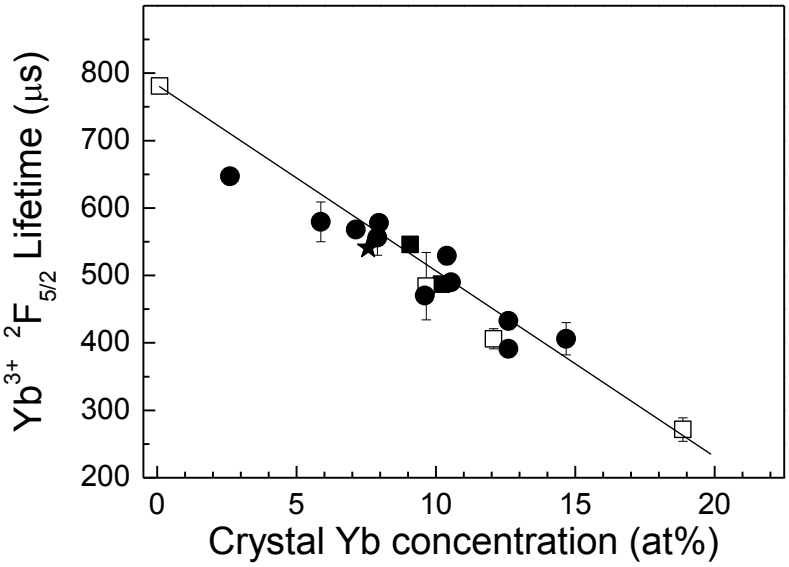

Figure ESI.15. Evolution of the 300K Yb^{3+} $^2F_{5/2}$ lifetime with Yb concentration in Yb:CNGG-type crystals. The open symbols correspond to crystals grown with 99.9% purity of Yb_2O_3 and full symbols to those grown with ≥99.99% purity. λ_{EXC}= 971-972 nm. λ_{EMI}= 1021-1035 nm. Squares are for Yb:CNGG, circles for Yb:CNNGG and stars for Yb:CLNGG. The line is a visual help.

xi) Comparative cw laser performance

As discussed in the main text, the use of low purity $CaCO_3$ for crystal growth induces crystal coloration, but this has not a strong impact on laser performance. This was shown in Figure 8 of the main text for a Yb:CNGG crystal. Figure ESI.16 extends these results to Na and Li modified Yb:CNGG-type single crystals.

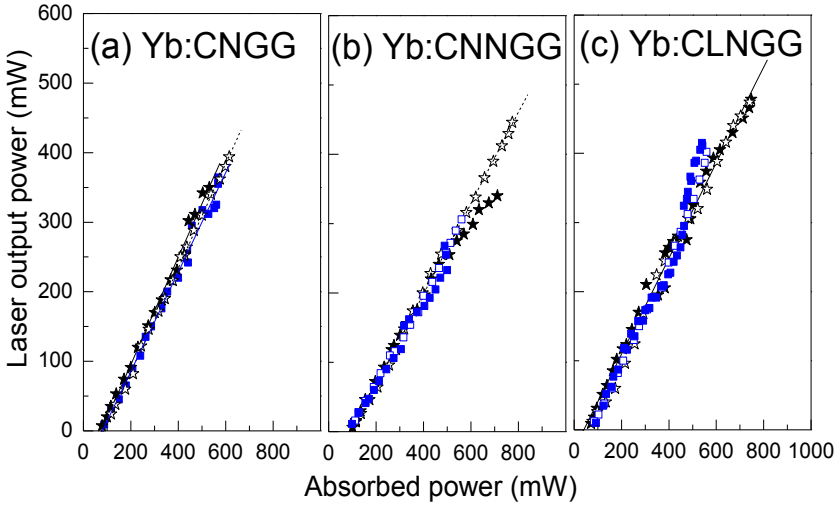

Figure ESI.16. Input-output cw laser characteristics of Yb:CNGG-type crystals grown by using 99.99% (black stars) or 99.5% (blue squares) $CaCO_3$ purity. 99.99% Yb_2O_3 purity was used in all cases. Full and open symbols are for cw and qcw laser operation, respectively. T_{OC}=10%. Lines are the best linear fits of the experimental results. (a) 9.01 at% Yb:CNGG crystal grown with 99.99% $CaCO_3$, d= 0.853 mm, λ_{EXC}= 971.9 nm, *vs* 9.08 at% Yb:CNGG crystal grown with 99.5% $CaCO_3$, d= 0.887 mm, λ_{EXC}= 971.6 nm. (b) 2.26% Na-modified 8.77 at% Yb:CNNGG crystal grown with 99.99% $CaCO_3$, d= 0.828 mm, λ_{EXC}= 971.6 nm, *vs* 2.3 at% Na-modified 9.6 at% Yb:CNNGG crystal grown with 99.5% $CaCO_3$, d= 0.840 mm, λ_{EXC}= 971.6 nm. (c) Li-modified 7.28 at% Yb:CLNGG crystal grown with 99.99% $CaCO_3$, d= 0.824 mm, λ_{EXC}= 972.2 nm, *vs* Li-modified 7.57 at% Yb:CLNGG crystal grown with 99.5% $CaCO_3$, d= 0.831 mm, λ_{EXC}= 972.5 nm.

xii) Effect of air annealing on Yb^{3+} lifetime

In the literature CNGG crystal coloration is often ascribed to oxygen deficiency in the crystal produced by the use of reductive atmospheres during the growth, in most cases this atmosphere was required to preserve used Ir crucibles. It is assumed that crystal oxygen stoichiometry is restored by air annealing near the melting point. Although all our crystals were grown using platinum crucibles in an oxygen rich atmosphere, we have tested the effect of such annealing in an attempt to improve the radiative properties of Yb:CNGG-type crystals.

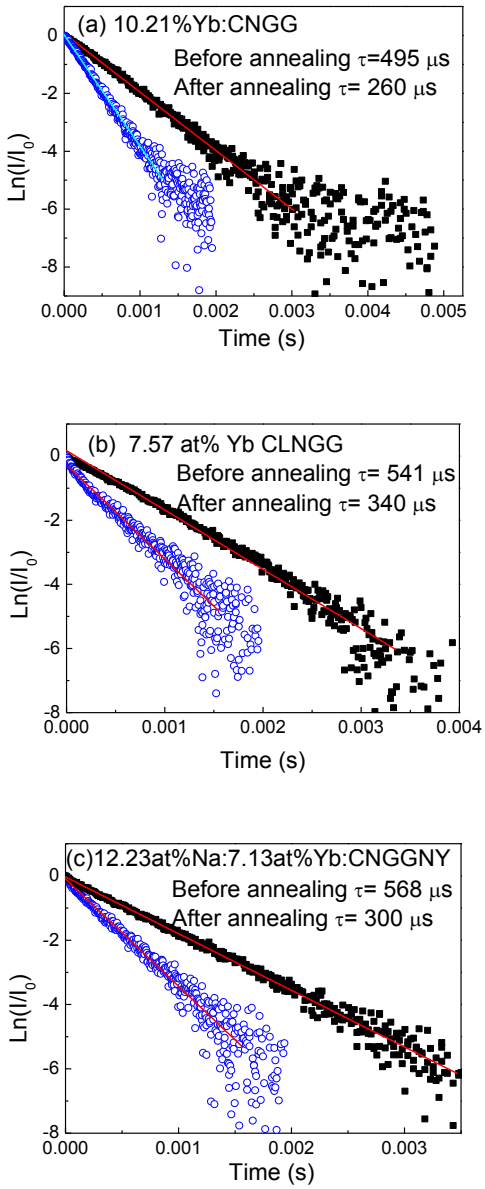

Figure ESI.17. Fluorescence time decay of Yb:CNGG-type ground crystals. As grown crystals, full symbols. After 1150 °C air annealing, open symbols. (a) Yb:CNGG. (b) Yb:CLNGG. (c) Yb:CNNGG.

For this purpose the crystals were ground to ease the oxygen diffusion by increasing the surface/volume ratio. We chose to measure the Yb^{3+} lifetime as a parameter sensitive to the presence of color centers and other point defects. Samples of all available Yb:CNGG-type crystals were heated to 1150 °C for one week in an air flow. Figure ESI.17 shows selected results. In no case the Yb^{3+} lifetime increases with regards to the as-grown crystals, contrary a reduction of the lifetime is observed as a consequence of the annealing, showing that such annealing introduces further defect in the crystal, most likely due to the surface gallium volatility.

[1] B. Cockayne, "Czochralski growth of oxide single crystals. Iridium crucibles and their use" Platinum Metals Rev. 18(3), 86-91 (1974).
[2] A. A. Kaminskii, E. L. Belokoneva, A. V. Butashin, K. Kurbanov, A. A. Markosyan, B. V. Mill', O. K. Nikol'skaya, and S. E. Sarkisov, Inorg. Matter. 22(7) 927-936 (1987). [Translated from Neorg. Mater. 22(7), 1061-1071 (1986)].
[3] C. Coya, J. L. G. Fierro and C. Zaldo, "Thermal reduction of sillenite and eulite single crystals" J. Phys. Chem. Sol. 58(9), 1461-1467 (1997).
[4] C. Zaldo, M. J. Martín, C. Coya, K. Polgar, A. Péter and J. Paitz, "Optical properties of $MgNb_2O_6$ single crystals: a comparison with $LiNbO_3$" J. Phys.: Cond. Mater 7, 2249-2257 (1995).
[5] A. García-Cabañes, J. A. Sanz-García, J. M. Cabrera, F. Agulló-López, C. Zaldo, R. Pareja, K. Polgár, K. Raksányi and I. Fölvari, "Influence of stoichiometry on defect-related phenomena in $LiNbO_3$" Phys. Rev. B 37(11), 6085-6091 (1988).
[6] M. J. Martín, D. Bravo, R. Solé, F. Díaz, F. J. López and C. Zaldo, "Thermal reduction of $KTiOPO_4$ single crystals", J. Appl. Phys. 76(11), 7510-7518 (1994).
[7] A. Schmidt, S. Rivier, V. Petrov, U. Griebner. X. Han, J. M. Cano-Torres, A. García-Cortés, M. D. Serrano, C. Cascales and C. Zaldo, J. Opt. Soc. Am. B 25(8), 1341-1349 (2008).
[8] A. Méndez-Blas, M. Rico, V. Volkov, C. Cascales, C. Zaldo, C. Coya, A. Kling and L.C. Alves, J. Phys.:Cond. Matter 16, 2139-2160 (2004).
[9] V. Volkov, M. Rico, A. Méndez-Blas and C. Zaldo, "Preparation and properties of disordered $NaBi(XO_4)_2$, X=W or Mo, crystals doped with rare earths", J. Phys. Chem. Sol. 63, 95-105 (2002).